Molecular Vision 2003; 9:60-73 <http://www.molvis.org/molvis/v9/a10>
Received 31 December 2002 | Accepted 26 February 2003 | Published 11 March 2003

Three-dimensional analysis of mouse rod and cone mitochondrial cristae architecture: Bioenergetic and functional implications

Guy A. Perkins,[1,2] Mark H. Ellisman,[1,2] Donald A. Fox[3,4,5]

[1]Department of Neurosciences and [2]National Center for Microscopy and Imaging Research, University of California San Diego, La Jolla, CA; [3]College of Optometry, [4]Department of Biology and Biochemistry, and [5]Department of Pharmacology and Pharmaceutical Sciences, University of Houston, Houston, TX

Purpose: Comparative studies of structure related to function offer a promising means of understanding the significance of differences in cytoarchitecture. Mitochondrial crista structure is linked tightly to mitochondrial function. Non-foveal cone photoreceptors of primates contain considerably more inner segment mitochondria and have higher oxidative enzyme activity than do rods. In addition, it is suggested that light-adapted cones have a higher aerobic ATP demand than light-adapted rods. Therefore, we investigated the oxidative metabolism and three-dimensional membrane architecture of mouse rod and cone inner segment mitochondria.

Methods: We determined the number, size, cytochrome c oxidase (CO) reactivity, and membrane architecture of rod and middle wavelength-sensitive (M) cone inner segment mitochondria from 21 day old light-adapted C57BL/6 mice using conventional electron microscopy and the three-dimensional approach of single- and double-tilt electron microscope tomography. Fourteen different measurements of mitochondrial substructures were analyzed. Photoreceptor oxygen consumption was determined in dark- and light-adapted retinas.

Results: Rod and cone mitochondria displayed an orthodox conformation. Cone inner segments, compared to rods, contained 2-fold more mitochondria and were more CO reactive. Rod and cone mitochondria had similar outer-inner membrane width, contact site width, diameter and density, crista width, number of cristae/volume, number of cristae segments/volume, and fraction of cristae with multiple segments. In contrast, cone mitochondria had narrower crista junctions, greater cristae connectivity, and approximately 3-fold more cristae membrane surface area compared to rods. The increased cristae membrane surface area in cones was accomplished by connecting more cristae segments together, rather than by creating more cristae.

Conclusions: These results demonstrate that middle wavelength (M) cones have a different bioenergetic signature than do rods and suggest that the aerobic ATP demand and production is greater in light-adapted cones than in light-adapted rods. Cones utilize two complimentary strategies to increase their aerobic ATP production: increase the number of mitochondria and increase the cristae surface membrane area. The greater ATP generation by cones may also provide increased protection against metabolic insults and apoptosis compared to rods.

The basic structure, biochemistry and function of mammalian retinal rod and cone photoreceptors are well described [1-7]. Biochemical, physiological, and microscopy studies have established that 60-65% of retinal mitochondria are located in the photoreceptor inner segments, that the inner segments have the highest retinal cytochrome c oxidase (CO) activity (i.e., stain more intensely), and that photoreceptors have 2 to 3 fold greater oxygen consumption than the inner retina [8-14]. Although rod and cone photoreceptors share several common features and properties, many of their functions are significantly different. Compared to rods, cones are less sensitive to light, respond and recover more quickly, adapt over an extended range of luminance intensities, have higher relative permeability for Ca^{2+} in their outer segments (COSs), have a higher fraction of the dark current carried by Ca^{2+}, and express higher levels of the mitochondrial matrix enzyme ornithine aminotransferase (OAT) [9,15-21]. Moreover, in primate retinas the cone inner segments (CISs), except for the narrow CISs in the foveal region [14,22], have significantly more mitochondria, have higher CO activity, and stain more intensely for Na^+,K^+-ATPase than rod photoreceptor inner segments (RISs) [8,9,14]. These results suggest that cones are bioenergetically more active than rods and thus should produce more ATP than rods.

There are relatively few reports on the ultrastructural details of rod and cone mitochondria and even fewer on their comparative aspects [8,14,23-25]. One of the earliest ultrastructural studies of retinal mitochondria focused on guinea pig RISs and found that the major component of RISs was elongated and densely packed mitochondria [26]. In primates, CISs contain approximately 10 times more mitochondria than RISs and the mitochondrial volume density is approximately 60% in rod ellipsoids and approximately 80% in cone ellipsoids [8,14]. Prior to the finding that photoreceptors responded to light with graded potentials [6], Sjostrand [23] suggested that the relative number of mitochondria in rods and cones reflected a difference in the cells' mean frequency of discharge. Subsequently, Cohen [8] suggested that the cones had more

Correspondence to: Donald A. Fox, Ph.D., University of Houston, College of Optometry, 505 J. Davis Armistead Building, Houston, TX, 77204-2020; Phone: (713) 743-1964; FAX: (713) 743-2053; email: dafox@uh.edu

mitochondria because their energy requirements were significantly greater than those of rods, which is consistent with the above noted conclusion. More recently, it was suggested that the numerous cone mitochondria enhance the waveguide properties of cones [14]. To date, however, the three-dimensional (3-D) architecture of photoreceptor inner segment mitochondria and the relationship between the density and arrangement of cristae and mitochondrial bioenergetics has not been adequately studied.

The 3-D technique with the highest resolution available for studying mitochondria is electron microscope tomography [27-29]. Conventional transmission electron microscopy (TEM) played an early and essential role in formulating and shaping the concepts of mitochondrial bioenergetics [30-32]. More recently, the development and refinement of 3-D electron imaging using high-voltage electron tomography has provided significant new insights into mitochondrial bioenergetics as well as the ultrastructure and substructure of normal and apoptotic mitochondria [33-40]. The limitation of conventional TEM operating at 100 kV is that it only provides single images from ultrathin (50-100 nm thick) sections. This does not permit adequate sampling from mitochondria with dimensions that are typically 0.2 to 2 µm or resolution of mitochondrial substructures that range from 2-50 nm. In con-

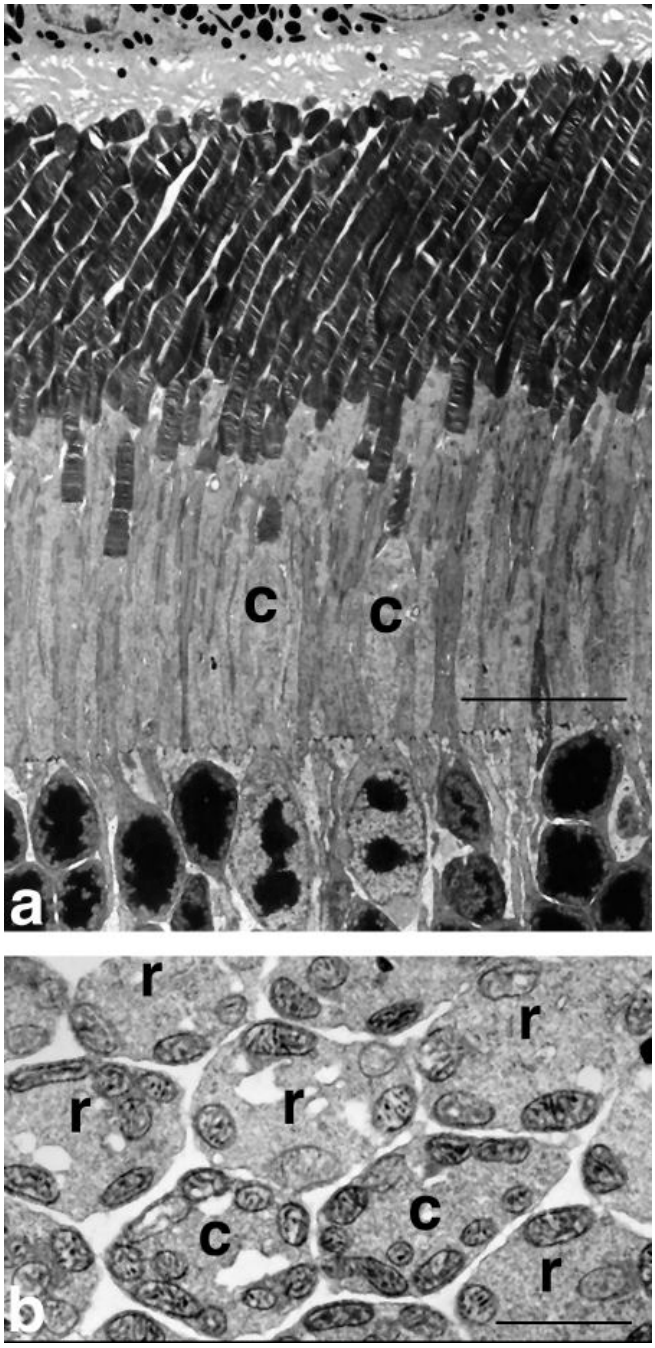

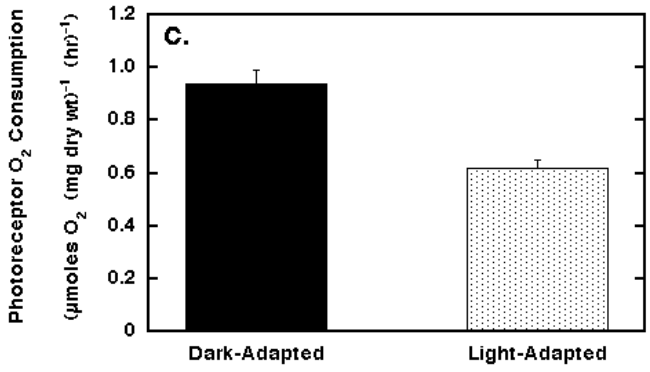

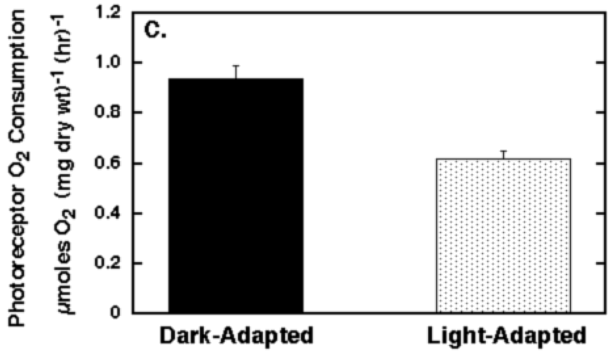

Figure 1. Electron microscopy and photoreceptor oxygen consumption of 21 day old mouse retina. Conventional electron micrographs of retinas and photoreceptor oxygen consumption (QO_{PR}) from postnatal day 21 mice. **A**: Electron micrographs of the rod (r) and cone (c) outer and inner segments and distal outer nuclear layer from superior temporal retina of a light-adapted mouse. Note that the tips of the middle wavelength-sensitive cone outer segments lie in the rod inner segment region. The cone inner segment diameter is approximately twice that of the rod inner segment. The cone nuclei are located in the distal portion of the outer nuclear layer and contain several clumps of irregularly shaped heterochromatin, whereas the rod nuclei contain a single compact mass of heterochromatin. Scale bar represents 10 µm. **B**: Transverse section through ellipsoid region of photoreceptor inner segment illustrating cytochrome oxidase stained rod (r) and cone (c) mitochondria. Note that there are approximately twice as many cone mitochondria per photoreceptor compared to rod photoreceptors and that the cone mitochondrial inner membranes stain more intensely for cytochrome oxidase than do the rods. Scale bar represents 1 µm. **C**: QO_{PR}. QO_{PR} was measured in pairs of dark-adapted and rod saturating light-adapted whole retinas from five mice.

trast, electron microscopy (EM) tomography utilizes thick sections (0.25-5.0 µm), microscopes operating at 400-3000 kV, multiple tilt-series usually ranging from -60° to +60°, and sophisticated computer algorithms for precise spatial localization [33,35,36,38].

Our goals were to determine, in light-adapted mouse retinas, the: (1) number of mitochondria and oxidative enzyme activity in RIS and CIS, (2) photoreceptor oxygen consumption (QO_{PR}) and compare it to that in dark-adapted photoreceptors, (3) dimensions and connectivity of RIS and CIS mitochondrial cristae and contact sites, and (4) structural motifs of RIS and CIS cristae. Here we show that mouse CIS, compared to RIS, mitochondria have: approximately 2-fold more mitochondria, higher oxidative enzyme staining, narrower crista junctions, greater cristae connectivity and approximately 3-fold more cristae membrane surface area. The implications for mitochondrial ATP generation and response to metabolic dysfunction are discussed.

METHODS

Materials: All chemicals were analytical or molecular biology grade and were purchased from Sigma Chemical Co. (St. Louis, MO) or Fisher Scientific (Pittsburgh, PA) unless otherwise noted.

Experimental animals and retinal fixation: All experimental and animal care procedures were in compliance with the principles of the American Physiological Society, the NIH Guide for the Care and Use of Laboratory Animals and Maintenance (NIH publication No. 85-123, 1985) and were approved by the Institutional Animal Care Committee of the University of Houston. C57BL/6 mice (Harlan Sprague Dawley, Indianapolis, IN) were housed in a room maintained at 22 ± 1 °C with a 12:12 h light dark cycle and cage illumination of 5-10 lux. Mice were mated and upon giving birth, postnatal day 0, the litters were culled to eight pups. Only female mice were used in order to directly compare our present results with previous results [39,41-44].

On postnatal day 21 (weaning), two hours after light onset, the mice were sacrificed by decapitation. The eyes were

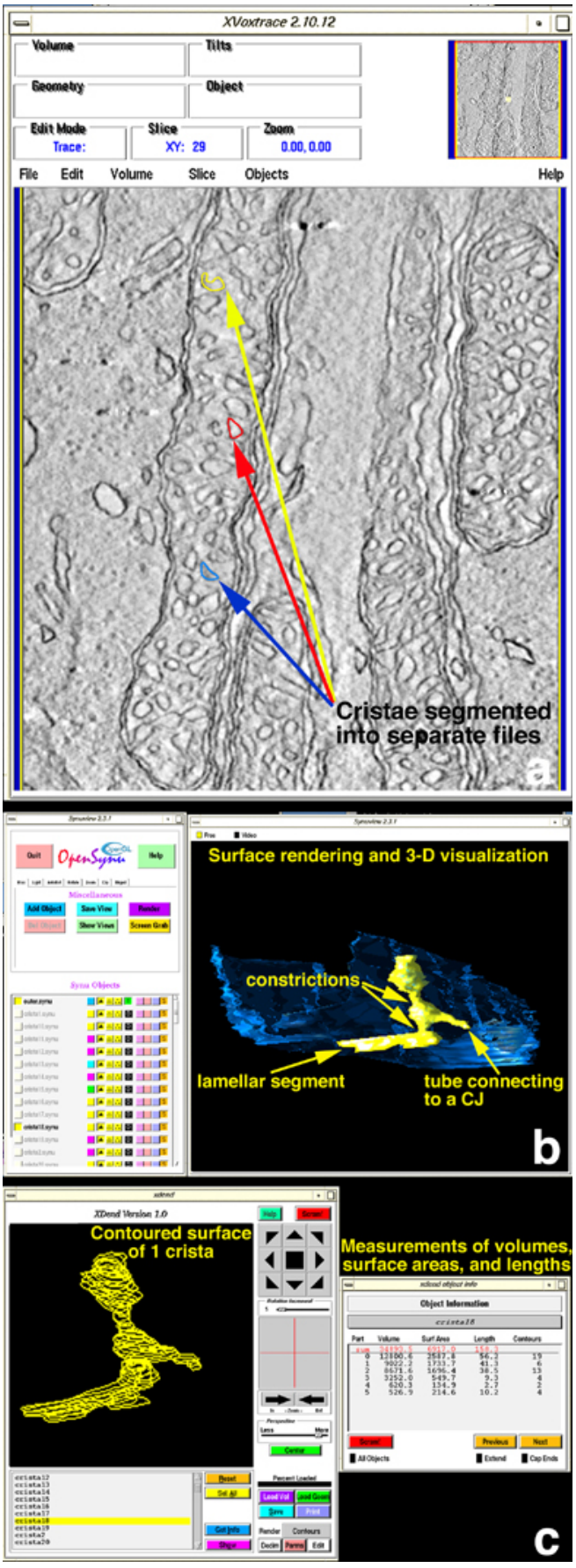

Figure 2. Quantitative analysis of mitochondrial substructures. **A**: Use of XVoxtrace. The software program XVoxtrace allows volume segmentation, as shown here for a cone mitochondrion. Segmentation is based on membrane topography and separates individual cristae, inner boundary and outer membranes. The separate tracings of three cristae are shown in yellow, red and blue. **B**: Use of Synuview. Using the software program Synuview, individual or any combination of cristae surfaced-rendered can be displayed in order to visualize their 3-D shapes and membrane architecture in user-defined orientations. This program was used to classify the structural motifs of lamellae, tubes, crista junctions, and constrictions. A crista showing all of these elements is displayed in yellow. The outer membrane is shown in blue. **C**: Use of XDend. Measurements of surface-rendered elements permitted a comparison of substructures inside mitochondria using the program XDend. A contoured crista is shown on the left. On the right, a table of numerical values associated with volume, surface area, length, and number of contours is displayed for the crista on the left.

removed and fixed by immersion in ice-cold 3% glutaraldehyde, 2% paraformaldehyde and 0.1% $CaCl_2$ in 0.1 M cacodylate buffer (pH 7.4) without or with (only for CO histochemistry) 4% sucrose. As described [41], the superior portion of the eye was identified with a suture, the corneas were cut at the limbus and each eye was placed in 15 ml of the same fresh fixative for either 2 h (for CO histochemistry) or overnight at 4 °C for conventional EM and EM tomography.

For all experiments, the superior temporal retina, 200-250 µm from the optic nerve head, was used because it contains almost exclusively middle wavelength-sensitive (M) cones [45]. We wanted to compare these middle wavelength-sensitive cones, which are similar to those in other mammals [45,46], to rods. The number and distribution pattern of middle wavelength-sensitive cones is adult-like by postnatal day 14 and is similar in male and female mice [45].

Conventional EM and CO histochemistry: For conventional EM, each fixed eye was placed in fresh ice-cold buffer and the superior temporal quadrant near the optic nerve (central retina) was trimmed. The retinal sections were dehydrated and embedded in Spurrs resin as described [44]. Ultra-thin longitudinal sections of the whole retina and transverse sections through the RIS and CIS were stained with uranyl acetate and lead before being examined in a JEOL 100-C or 1200EX transmission electron microscope (Tokyo, Japan). The number of mitochondria per cross-section of RIS and CIS was obtained from 10-30 photoreceptors from each of five different mice. The mean number from each mouse was determined and then an overall mean ± SEM was calculated (n=5).

For CO histochemistry, the cornea, lens and vitreous were removed and the eyecups were cryoprotected in 30% sucrose at 4 °C for an additional 24 h. The retinas were quick frozen, 15-25 µm sections were cut on a microtome, incubated, histochemically reacted for CO, and the superior temporal retinal sections processed for EM examination as described [47,48]. The differences in staining intensity between rod and cone mitochondria were evaluated qualitatively on transverse sections through the RIS and CIS of four different mice. The specificity of the cytochemical reaction was determined by adding 10 mM KCN to the incubation buffer, which completely eliminated any CO reaction product in the mitochondria (data not shown).

Photoreceptor oxygen consumption: QO_{PR} was recorded from retinas isolated from postnatal day 25 mouse retinas. Both retinas were placed in the recording chamber at the same time. QO_{PR} was determined polarographically and recorded continu-

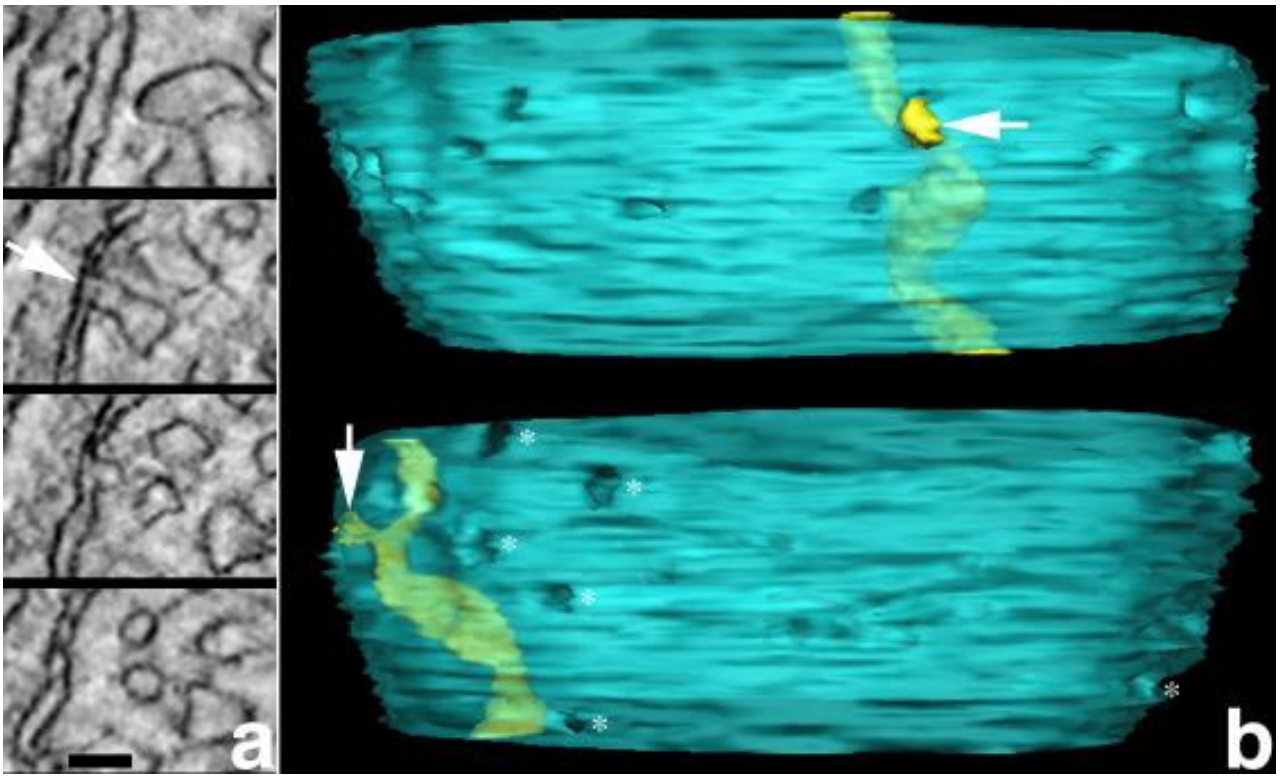

Figure 3. Perpendicular extensions connect tubular cristae. This figure demonstrates that tubular cristae in cone mitochondria connect to the inner boundary membrane through perpendicular extensions from the tubular shaft. **A**: Serial slices through the tomographic reconstruction of a cone mitochondrion. The serial slices illustrate how the crista membrane extends from the tubular shaft towards the periphery of the mitochondrion, forms a crista junction (arrow) and finally contracts away from the boundary membrane. Scale bar represents 50 nm. **B**: Volume segmentation and surface rendering of the same crista. The two 90° rotation views (top and bottom) highlight the dimensions of the crista junction opening (arrows) in relation to the crista (yellow) and mitochondrial inner membrane (blue). Crista junctions (*) from other cristae also are shown and are indicated by fenestrations in the inner membrane. These fenestrations accurately portray the size and variation in dimensions of these junctions.

ously in the dark or during presentation of a rod-saturating light adapting stimulus as described [12,49]. The mean dry weight of each retina was 0.55 mg.

EM tomography: Single-tilt series: For EM tomography, the superior temporal quadrant retinal sections were dehydrated, embedded in Durcupan resin and imaged in situ using the techniques described by Perkins and co-workers [33,34]. 3-D reconstructions were obtained from semi-thick samples (approximately 500 nm) in a tilt-series every 2° from -60° to +60° on a JOEL 4000EX electron microscope operated at 400 kV. Fourteen different types of measurements of mitochondrial substructures were obtained with large sampling sizes: (1) outer membrane to inner (OM-IM) widths, (2) cristae widths, (3) cristae junction diameters, (4) contact site widths, (5) contact site diameters, (6) classical contact site density, (7) bridge contact site density, (8) number of cristae segments per mitochondrial volume, (9) number of cristae per mitochondrial volume, (10) cristae volume per mitochondrial volume, (11) fraction of cristae with multiple segments, (12) cristae surface area per mitochondrial surface area, (13) number of cristae segments per crista, and (14) number of constrictions per crista. Overall, measurements from tomographic reconstructions were made from 28 distinct mitochondria (14 from rods and 14 from cones) using retinas from four different mice.

EM tomography: double-tilt series: Double-tilt tomography improves the accurate reconstruction of the 3-D organization of complex biological structures [50]. The most recognized advantage of double-tilt reconstruction is the improved resolution in the Z-dimension (perpendicular to the specimen plane). A second, less-appreciated advantage is that, unlike single-tilt tomography, double-tilt tomography provides optimal resolution for elongated structures, such as tubular cristae, at any orientation in the specimen. A third advantage is the capability to correct distortions that arise during the acquisition of images. For example, if the specimen shrinks nonuniformly during image collection, the resultant distortions can be corrected more effectively during registration of two related reconstructions than during alignment of the respective tilt series.

Double-tilt tomography was performed by first collecting two tilt series around orthogonal axes. After the first tilt series was complete, the specimen grid was rotated 90° and

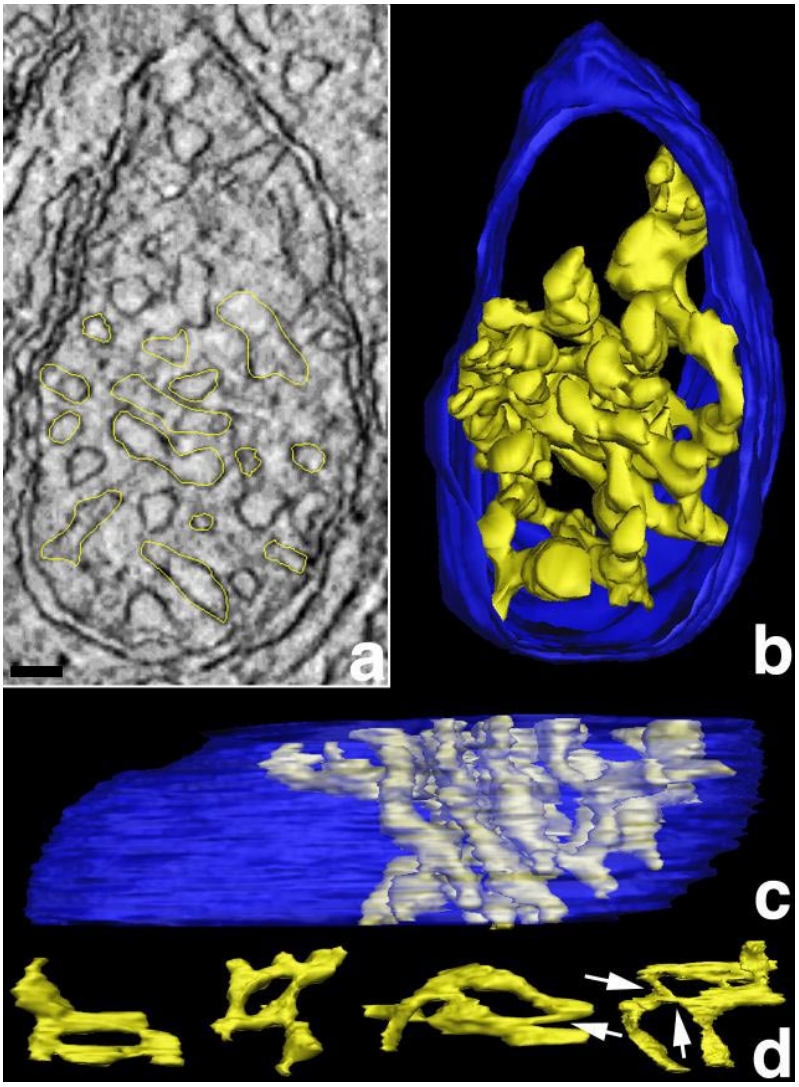

Figure 4. Cone mitochondria have high cristae connectivity. **A**: Slice through a cone mitochondrion with one traced crista. Connectivity is defined as the sum of continuous connections of cristae segments with each other that form a complete crista. In other words, the connection of well-defined cristae shapes, such as tubes and lamellae, is determined in 3-D. Electron tomography provided this 3-D mapping analysis, which is not feasible with conventional electron microscopy of thin sections. In one 2.2 nm slice of the volume (shown), the yellow tracings highlight all the branches of the largest crista that has the most segments and constrictions of all the cone mitochondrial reconstructions. The connectivity was best mapped after the volume was segmented and surface-rendered. Scale bar represents 50 nm. **B** and **C**: Perpendicular views after segmentation of the crista. The crista, traced in A, is shown in yellow. It appears almost maze-like because of its great connectivity of more than 20 segments. The outer membrane is shown in blue. This largest crista measured in cone mitochondria extends through roughly half of the cone mitochondrial volume, has a volume of 110,000 nm^3, which represents approximately 9% of the entire mitochondrial volume, and has an inner membrane surface area of 490,000 nm^2, which is equivalent to 97% of its total outer membrane surface area. This same connectivity and extent was not observed in rod mitochondria (Figure 5). **D**: "Loop" connectivity. An unusual crista architecture in cone mitochondria was observed that was rarely noted in rod mitochondria. This architecture is described as loop connectivity because of the connection of crista segments following a closed pathway through the intracristal space back to each other rather than to the inner boundary membrane. Four loops from different cone mitochondria are illustrated. The arrows indicate the narrow connections (constrictions) between loop segments.

the second tilt series was acquired. Separate tomographic reconstructions were computed from each tilt series. The IMOD software suite was used to process the images in each tilt series [50]. Each perpendicular tilt series was aligned separately using 10-nm gold particles placed on both surfaces of the section. The positions of more than a dozen particles were marked on the 0°image using the modeling option. A bead-tracking seed program searched for the position of each gold particle on each image of the tilt series. The computer-generated model of particle positions was examined with the beadfixer package and the incorrect positions, or failures to track a particle past a certain image, were corrected. After alignment, the tomographic reconstruction was generated by R-weighted back-projection.

Computational merging of the two single-axis reconstructions was accomplished with a warping procedure [50]. A series of local linear transformations allows one to correct even nonlinear distortions and thus warp one reconstruction to the other. First, multiple linear regression was used to match fiducial marks between the two volumes. Then, 3-D cross-correlation between patches from the two volumes determined displacements that were used in another regression to obtain a refining 3-D transformation. Densities were linearly scaled to match between volumes. The combination of volumes was conducted in Fourier space. The 3-D Fourier transform of each volume was computed and for every point containing data from both volumes, the values were averaged. Otherwise, the values from one or the other volume were used. The inverse of this composite Fourier transform provided the final combined volume.

Statistical analysis: All group data were analyzed by two-tailed Student's t-test. All data are presented as means ± SEM. For all data, the difference between rods and cones was regarded as significant if $p<0.05$.

RESULTS

Conventional EM and CO histochemistry: Rods comprise approximately 96% of the total photoreceptor population in C57BL/6 mice [24,44]. In longitudinal sections, the rod and cone photoreceptors were distinguished by their morphological differences (Figure 1A: also see [24,41,44]). The CISs are larger (3-4 μm diameter) and more electron-lucent than RISs (approximately 2 μm diameter). The cone nuclei are located in the outer third of the outer nuclear layer, are mostly oval,

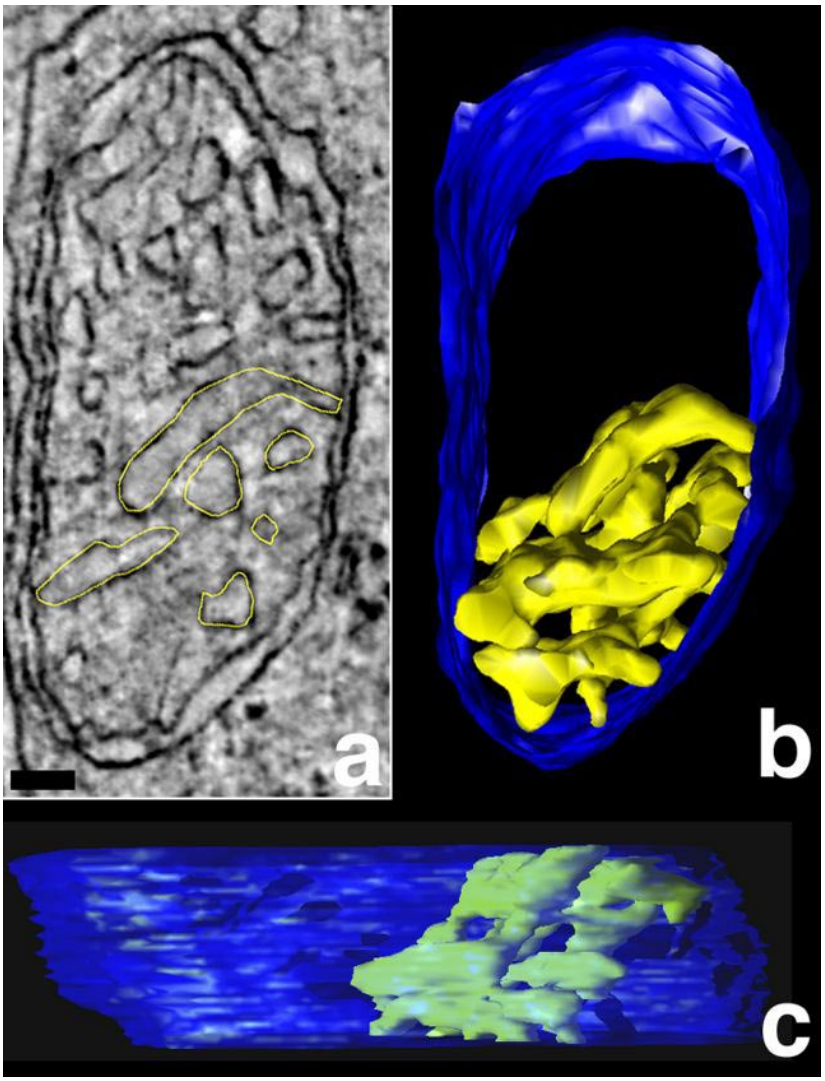

Figure 5. Rod mitochondria have both tubular and lamellar cristae segments. **A**: Slice through a rod mitochondrion reconstructed in 3-D. A similar analysis as conducted with cone mitochondria (Figure 4) was performed with rod mitochondria. A 3-D analysis is needed to determine which membrane profiles are separate cristae and which profiles represent slices through branches of the same crista. The yellow tracings highlight the branches of the largest crista in this slice through the rod mitochondrial volume. Note that four branches have a tubular profile, whereas two branches have a lamellar profile. Scale bar represents 50 nm. **B** and **C**: Perpendicular views after segmentation of the crista. The crista, traced in **A**, is shown in yellow and the outer membrane is shown in blue. This largest crista measured in rod mitochondria has a volume of 51,000 nm^3, which represents approximately 7% of the entire mitochondrial volume, and has an inner membrane surface area of 170,000 nm^2, which is equivalent to 51% of its total outer membrane surface area. Note that these values are considerably smaller than those for the largest crista measured in a cone mitochondrion (Figure 4). Hence, rod mitochondria possess moderate crista connectivity as opposed to the rather high connectivity measured in cone mitochondria.

and appear to contain several clumps of irregularly shaped heterochromatin. The rod nuclei are rounder and contain a single compact mass of heterochromatin. In addition, although less frequently observed, the COSs are thinner and shorter than ROSs, and are located relatively deep in the RIS region (Figure 1A).

In transverse sections, RISs and CISs of mice are most readily distinguished by a difference in the number of mitochondria. Rods have 5.2 ± 0.3 mitochondria per cell (mitochondrial density), whereas cones possess 10.1 ± 0.2 mitochondria per cell (Figure 1B). It appears that CISs accommodate this two-fold increase in mitochondrial density by increasing their cross-sectional area two- to four-fold since the overall dimensions of the rod and cone mitochondria are not significantly different. We observed that the most intense CO staining in the light-adapted mouse retina occurred in photoreceptor inner segments (data not shown) and that cone mitochondria were more uniformly stained and more reactive than rod mitochondria (Figure 1B). These findings are consistent with reports for other light-adapted mammalian retinas [9,10]. These results suggest that middle wavelength (M) cones have a different bioenergetic signature than do rods and that the aerobic ATP generation in cones is greater than in rods.

Photoreceptor oxygen consumption (QO_{PR}): The dark-adapted QO_{PR} of isolated retinas was 0.94 µmole O_2 mg dry wt^{-1} hr^{-1} and it decreased approximately 35% during light ad-

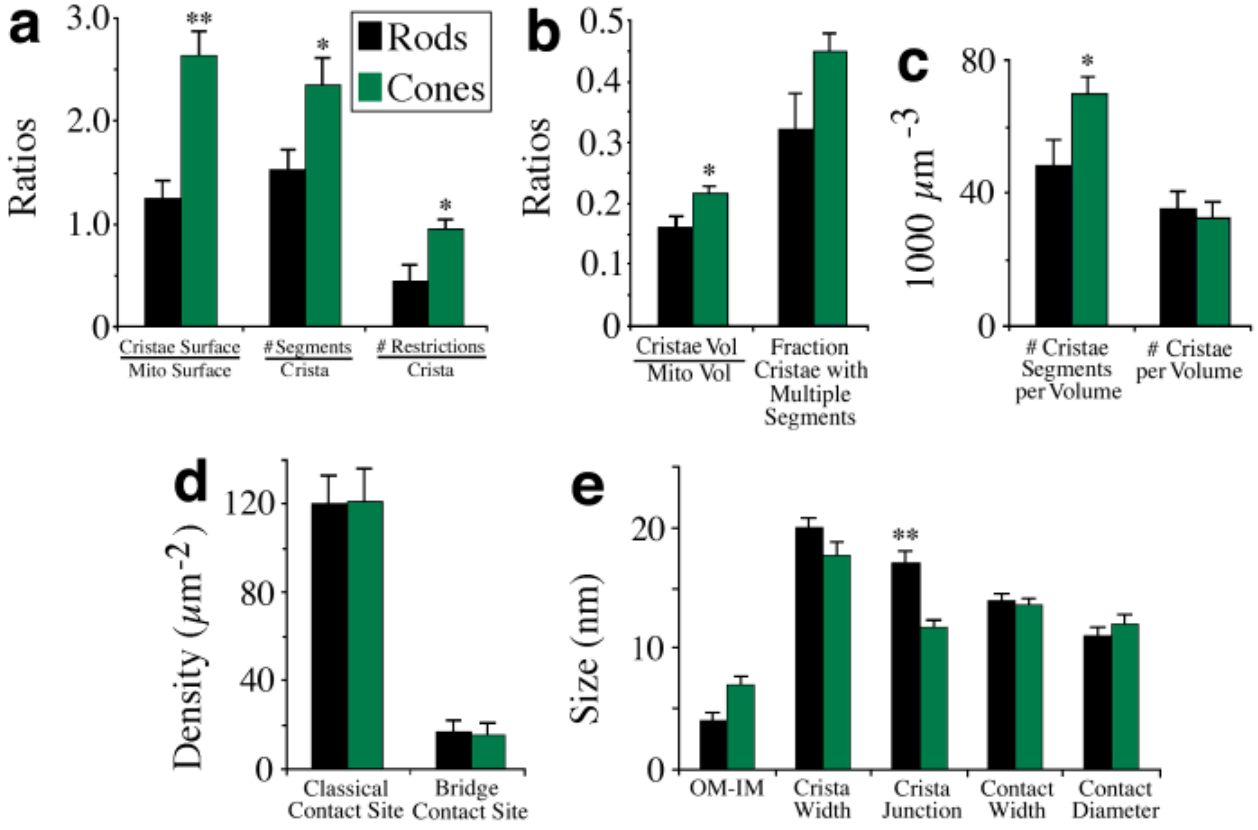

Figure 6. Substructure measurements of rod and cone mitochondria from 3-D tomographic reconstructions. Measurements were conducted, using the NIH Image program, on the tomographic reconstructions from seven rods and seven cones from four different mice on equally spaced slices through their volumes. The histograms represent means ± SEMs. A two-tailed Student's t-test was used to determine significant differences: *p < 0.05; **p < 0.005. **A**, **B**, and **C**: Comparison of cristae measurements. The reconstructed portion of the mitochondrion was segmented along membranes: outer membrane, inner boundary membrane and cristae membranes. The program XDend calculated the volume and surface area values for the outer membrane (used for "mito" in the denominator) and each crista. The values for individual cristae were summed to provide the numerator of the ratios (a and b) or number per volume **C**. Examples of "segments" and "constrictions" are shown in Figure 2. **D**: Surface density of contact site classes. Contact sites were divided into two classes: classical and bridge. The classical contact site is where the outer and inner boundary membranes join together, whereas the bridge contact site spans across the intermembrane space (forms a bridge) without a change in distance between the outer and inner membranes [52]. **E**: Size of mitochondrial substructures. The outer to inner membrane distance was measured perpendicular to the membranes, from the outer edge of the outer membrane through to the inner edge of the inner membrane at randomly selected points along the periphery that were not contact sites. The contact width was measured perpendicular to the membranes, from the outer edge of the outer membrane through to the inner edge of the inner membrane. The contact diameter was measured parallel to the membranes. The crista junction is the largest opening at sites where the inner boundary membrane involutes into the interior. The crista width is the width of the intracristal space at randomly selected points along cristae at sites other than junctions. All sizes are in nanometers (nm).

aptation to a rod-saturating stimulus (Figure 1C). These measurements predominantly reflect the rod QO_{PR} because the mouse retina contains approximately 96% rods [24,45]. This conclusion is consistent with our QO_{PR} measurements in isolated rat retinas and isolated rat rod photoreceptors [12,49]. Similar light-induced decreases in QO_{PR} were observed in the rod-dominant parafoveal region of anesthetized primates [51].

3-D structure of rod and cone mitochondria: A quantitative analysis, using tools developed for electron tomography, was performed on the mitochondrial reconstructions from rods and cones. Volume segmentation was utilized to analyze individual cristae (Figure 2A). Their 3-D shapes and membrane architecture were visualized in varying orientations to classify the structural motifs of lamellae, tubes and constrictions (narrow connections between crista segments) per each crista (Figure 2B). Surface rendering and measurements of volume and surface elements permitted a comparison of substructures inside mitochondria (Figure 2C). Because of the complex membrane topology of rod and cone cristae, which usually possess multiple shape elements in each crista, an analysis of the architecture of individual crista could only have been performed with the 3-D information provided by electron tomography. We found that most cristae had both lamellar and tubular segments usually with restricted openings placed along their lengths as emphasized in Figure 2B. Although, some cristae were tubular throughout their length, it was rare to find a crista that was exclusively lamellar.

We discovered that most tubular cristae in rod and cone mitochondria connect to the inner boundary membrane not end-to-end, as one might expect from a tubular structure, but through perpendicular extensions from the tubular shaft. Figure 3A displays serial slices through the tomographic reconstruction of a typical cone mitochondrion that shows how the crista membrane extends from the tubular shaft towards the periphery of the mitochondrion, forms a crista junction and finally contracts away from the boundary membrane. Figure 3B shows the same crista after volume segmentation in relation to the inner boundary membrane. The two 90° rotation views highlight the perpendicular extension of the crista membrane that ends in a crista junction and the dimensions of the opening into the intermembrane space.

Cone mitochondria have approximately 1.5-fold greater cristae connectivity than do their rod counterparts (Figure 4, Figure 5, and Figure 6A). By “connectivity”, we mean the continuous connection of cristae segments with each other to form a complete crista. Figure 4 presents an example of a crista from a cone mitochondrion with extensive connectivity that appears almost maze-like. When viewing an image from a thin section or a slice through the tomographic reconstruction, one might interpret the cristae profiles as representing separate cristae (Figure 4A and Figure 5A). However, instead of being separate cristae, many of these profiles represent slices through branches of the same crista, as those traced in cone mitochondria (Figure 4A) and rod mitochondria (Figure 5A) all belong to one crista. The connectivity was mapped after each volume was segmented and surface-rendered. Only electron tomography with its inherent 3-D nature can provide this kind of mapping analysis. Figure 4B,C and Figure 5B,C show perpendicular views of the segmented crista traced in Figure 4A and Figure 5A, respectively. The crista in the cone mitochondria has more than 20 segments, which extends through half of the cone mitochondrial volume (Figure 4). Such connectivity and extent was not observed in rod mitochondria, although these organelles possess moderate crista connectivity (Figure 5). We also observed unusual crista architecture in cone mitochondria that was rarely observed in rod mitochondria; this being the connection of crista segments back to each other rather than to the inner boundary membrane. This conformation might be described as “loop” connectivity because one can follow a closed pathway through the intracristal space without connecting to a crista junction. Figure 4D illustrates four such loops from different mitochondria and also shows narrow connections, as small as 6 nm, between loop segments. The loop connectivity found in cone mitochondria differs from the connectivity observed in all other tomographic reconstructions of this

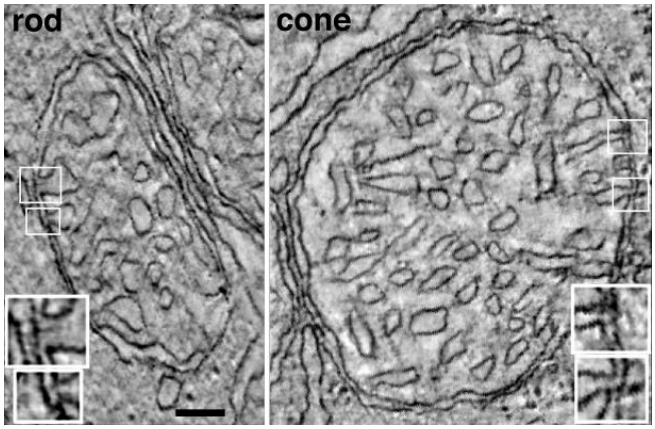

Figure 7. Slices through mitochondria from rod and cone tomographic reconstructions. These slices show the expected orthodox conformation in situ. Each slice is 2.2 nm thick. Examples of the mitochondrial crista junctions are boxed. The insets are shown at twice the normal magnification and emphasize the variation in the widths of openings within and between each photoreceptor cell type. Scale bar represents 100 nm.

Table 1. Mitochondrial crista junction diameter in rod and cone photoreceptor inner segments and central nervous system neurons

Cell Type	Number of Measurements	Mean Cristae Junction Opening (nm)	Standard Deviation (nm)
Rods	212	17	6
Cones	31	12	4
Cerebellar Purkinje neurons	85	14	5
Striatal spiny neurons	43	14	4
Hippocampal CA1 pyramidal neurons	38	14	4
Cortical neurons	26	14	5

Comparisons of cristae junction diameters in rod and cone inner segment mitochondria with those in neurons from several different rat brain regions reveal that rod mitochondria have larger openings and cone mitochondria have smaller openings than do neuronal brain mitochondria. Cone mitochondria have a 30% smaller crista junction opening compared to those in rods. Data for the rods are from reference [39]. Data for the cones are from this paper. Data for the neuronal regions are from reference [52].

organelle in different cells, including neuronal mitochondria [33,52]. In contrast, constrictions within cristae are commonly observed in other cells [53,54]. However, cone mitochondria have a 2-fold greater number of constrictions per crista than do rods (Figure 6A).

The abundance of cristae membrane is significantly greater in cone mitochondria compared to the rod organelle. Because mitochondria are pleiomorphic structures, absolute volumes and surface areas do not provide an adequate comparison between photoreceptor cell types. However, ratios do. Variations in cristae surface area may be a consequence of structural differences of the cristae membranes themselves (lamellar or tubular) or as a difference in the density of their packing. We found that cone mitochondria have approximately 3-fold more cristae/mitochondrial membrane surface area than do their rod counterparts (Figure 6A). The volume occupied by cone cristae is 1.4-fold larger than that of rod cristae although the fraction of cristae with multiple segments (Figure 6B) and the number of cristae per mitochondrial volume were not different between rod and cone mitochondria (Figure 6C). These values reflect the 1.5-fold larger number of cristae segments per volume of cone mitochondria more than a conversion from the tubular to lamellar form of cristae (Figure 6C). The number of cristae segments per unit mitochondrial volume is greater in cones (Figure 6C) as is the number of segments per crista (Figure 6A). However, the number of cristae per unit mitochondrial volume is not (Figure 6C). These findings indicate that cone mitochondria accommodate their greater amount of inner membrane by connecting cristae segments together rather than by creating numerically more cristae. This is consistent with the observations presented above (Figure 4).

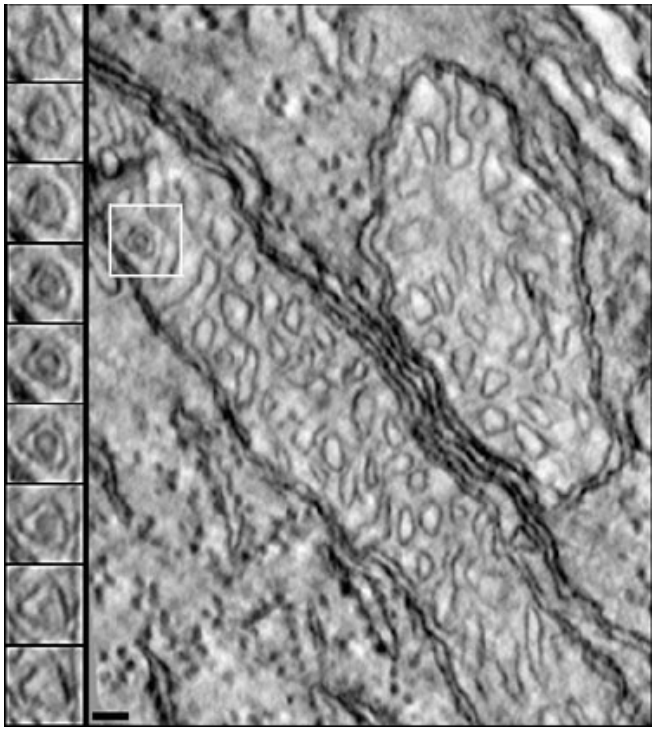

Figure 8. Unusual topography of a small matrix area completely surrounded by a crista. Because the matrix space is entirely bounded by a crista membrane, it is separated topographically from the mitochondrial periphery. This anomaly may be a structural defect or a viable, functioning unit. The multiple insets on the left show an enlarged area from serial slices through the 3-D reconstruction of the boxed region of the cone mitochondrion shown on the right. Scale bar represents 50 nm.

In addition to the seven different substructural RIS and CIS mitochondrial features related to cristae and crista architecture, seven additional substructures related to the mitochondrial outer and inner membranes were analyzed using tomographic reconstructions (Figure 6D,E and Figure 7). The rod and cone mitochondria, observed in situ, were in the orthodox conformation (Figure 7): as previously noted for the in situ mouse rod mitochondria [39]. The orthodox conformation is characterized by a relatively large matrix volume and an inner boundary membrane closely apposed to the outer membrane with a relatively small space between them [30]. In contrast, photoreceptor mitochondria isolated from light-adapted rats were observed in both the orthodox and condensed conformation [43,55]. In addition to measuring the surface density of the much studied classical contact site, defined by the outer and inner boundary membranes pinching together, the surface density of bridge contact sites (bridges or spans across the intermembrane space without a change in distance between the outer and inner membranes: [52]) was measured (Figure 6D). Figure 7 shows slices from rod and cone tomographic reconstructions with examples of crista junctions that emphasize the variation in openings within and between mitochondria of each photoreceptor.

Unexpectedly, we discovered that cone mitochondria have a 30% smaller crista junction opening compared to those in rods (Figure 6E). A comparison of junction diameters in rods and cones with neurons in several different rat brain regions is presented in Table 1. The comparisons reveal that rod mitochondria have larger openings and cone mitochondria have smaller openings than do neuronal brain mitochondria. The six other mitochondrial substructures (i.e., outer membrane to inner membrane widths, crista widths, crista junction diameters, contact site widths, contact site diameters, classical contact site density and bridge contact site density) that were measured in mouse rods and cones revealed no significant differences. Our mean values for crista width in rods and cones (approximately 14 nm) is similar to those obtained for crista "diameter" in rat photoreceptor inner segment mitochondria prepared in a different way and analyzed using scanning EM [25]. However, these authors report that only tubular cristae were observed in photoreceptor mitochondria, in contrast to both lamellar and tubular segments reported and observed in mouse rods and cones by electron tomography [39]. This difference may be due to the limited 3-D nature of scanning EM.

An unusual crista/matrix relationship was observed inside cone mitochondria, but never inside the rod organelle. Figure 8 shows a small matrix area completely surrounded by a crista. This is the first reported observation of a matrix space that is entirely bounded by a crista membrane and thus sepa-

rated topographically from the mitochondrial periphery. Whether this anomaly is a structural defect or a viable, functioning unit is unknown. However, there is no known rationale that precludes this crista/matrix unit from contributing to ATP synthesis as long as the electron transport chain and adenine nucleotide transporter are present in the crista membrane.

DISCUSSION

Comparative studies of structure related to function offer a promising means of understanding the significance of differences in cytoarchitecture [56]. The results from this study show that mitochondria from middle wavelength-sensitive CISs of light-adapted mice, compared to RISs, are more numerous, have higher CO activity, possess a greater cristae surface area and have narrower crista junctions. These results lend strong support to the idea that rod and cone mitochondria have fundamental substructural and functional differences. The implications of our histochemical and quantitative structural results are three-fold. The first is that light-adapted middle wavelength-sensitive cones, compared to rods, produce more ATP because they have higher energy requirements. The second is that greater ATP production by cones may provide cones with increased protection against metabolic insults and apoptosis compared to rods. The third is that cones employ different substructural motifs from rods to accommodate their functional requirements. Our results do not obviate the suggestion by Hoang et al. [14] that the numerous cone mitochondria may also act to enhance the waveguide properties of cones.

Cells employ one or more different strategies to increase significantly their aerobic ATP production: increase the mitochondrial size, total number of mitochondria per cell, volume of mitochondria per cell, and/or surface area of mitochondrial cristae membranes [57]. These increases have been documented in a wide variety of cells during transitions between normal physiological states, pharmacological or toxicological challenge, and pathological or disease states. In addition, ATP production is positively correlated with increased mitochondrial CO activity since CO is an integral membrane protein of the inner mitochondrial membrane catalyzing the final step of oxidative metabolism [57,58]. Generally, an increase in mitochondrial size occurs during vitamin or trace metal deficiencies, metabolic defects or diseases, or chemical exposure. In contrast, an increase in the absolute number of mitochondria per cell, relative volume of mitochondria per cell and mitochondrial cristae surface area reflect the aerobic energy production capacity of a cell and are associated with normal physiological processes [57].

Do light-adapted cones have higher aerobic ATP production than do light-adapted rods? The following evidence suggests this. CIS mitochondria have greater CO activity than RIS mitochondria, cones contain 2-fold more mitochondria than rods, and CIS mitochondria possess an approximately 3-fold greater surface area than RIS mitochondria. These results are consistent with observations that the parafoveal CISs in light-adapted primate retinas have significantly more mitochondria and higher CO activity than RISs [8,9,14,22]. A direct comparison with foveal cones was not made since primate foveal cones have narrow CISs, an almost non-discernible ellipsoid containing minimal mitochondria, and correspondingly the fovea has lower oxygen consumption than the parafovea [22,51]. In addition, our results are consistent with EM studies that showed more ATP in dark- and light-adapted frog COS and CIS mitochondria than similar compartments in rods [59].

Although anaerobic glycolysis may provide enough ATP and GTP for cGMP turnover in dark-adapted rods and cones, cGMP turnover increases almost 5-fold during continuous illumination and this exceeds the glycolytic capacity of rods to produce ATP [60-62]. The cGMP turnover and ATP demand in cones are likely larger and faster because the fractional Ca^{2+} permeability in COSs is twice that of ROSs, cones respond and recover faster than rods, the $Na^{+}/Ca^{2+}(K^{+})$ exchanger in COS is 8-10 times faster than that in ROSs, cones express higher levels of the GTPase-activating protein (GAP) RGS9-1 (Regulator of G-protein Signaling 9), and cone visual pigment regenerates approximately 5 times faster than rhodopsin [16-18,21,63-65]. It has been suggested that the additional high-energy phosphates needed by the outer segments are obtained via the phosphocreatine shuttle transport between the inner and outer segment [5,62,66]. Moreover, we suggest that carbonic anhydrase, which is present in primate red and green (M) cones but not in rods or blue cones [67,68], is necessary to regulate the intracellular pH of cones following the increased and rapid hydrolysis of cGMP into 5'-GMP and H^{+}. Furthermore, over 50% of the oxidative energy generated by the photoreceptors is needed for Na^{+} transport by the inner segment Na^{+},K^{+}-ATPase [49,69]. Light-adapted CISs should require more ATP since they have significantly higher Na^{+},K^{+}-ATPase activity than RIS [20]. Taken together, these findings indicate that cones require, produce, and utilize more ATP than do rods. Our results suggest that cones adopted two complimentary strategies to increase aerobic ATP production: increase the number of mitochondria and increase the cristae surface membrane area.

A second implication of our results is that greater ATP production may provide cones with increased protection against metabolic insults and apoptosis compared to rods. This proposal is supported by pharmacological, immunohistochemical, molecular, and clinical studies. For example, the cones of monkeys survive the intravenous injection of iodoacetate whereas the rods are destroyed [70]. The endogenous cytoprotective mechanism of cones during and following iodoacetate exposure is unknown. Although rods and cones have similar GLUT-1-type transporters and glycolytic enzymes [62,71-73], the kinetics might differ. The latter is suggested by the observation that changes in glucose levels affects rod function more than cone function [74]. Moreover, it appears that cones can also utilize endogenous glycogen stores as an alternative source of glucose, whereas glycogen is not present in normal rods [73], albeit it is present in rods of aged, diabetic, or lead-exposed rats [41,75,76]. Although not directly related to mitochondrial ATP production, patients with gyrate atrophy, caused by mutations in the gene of the mitochondrial matrix enzyme ornithine aminotransferase, exhibit a progres-

sive peripheral-to-central visual loss [77]. Here the cones may be temporally spared because mitochondrial density and ornithine aminotransferase mRNA levels are significantly higher in the parafoveal region compared to the periphery [14,19,22]. These results suggest that pharmacological treatment, vitamins and supplements, dietary management and other therapeutic strategies that preserve mitochondrial function, and especially those that reduce mitochondrial ATP loss and/or enhance ATP production [78,79], may prolong or increase the survival of aging, injured and degenerating photoreceptors.

The third implication is that cones utilize different substructural motifs to facilitate their functional requirements. Our 3-D analysis of rod and cone membrane architecture, in combination with the numerical and size considerations, enabled us to assess the relationship between mitochondrial structure and function. In addition to having twice the number of mitochondria, CIS mitochondria have approximately 3-fold more cristae surface area. The arrangement of cone, and to a lesser extent rod, cristae is reminiscent of the retiform cristae described for canary striated muscle under certain conditions [57].

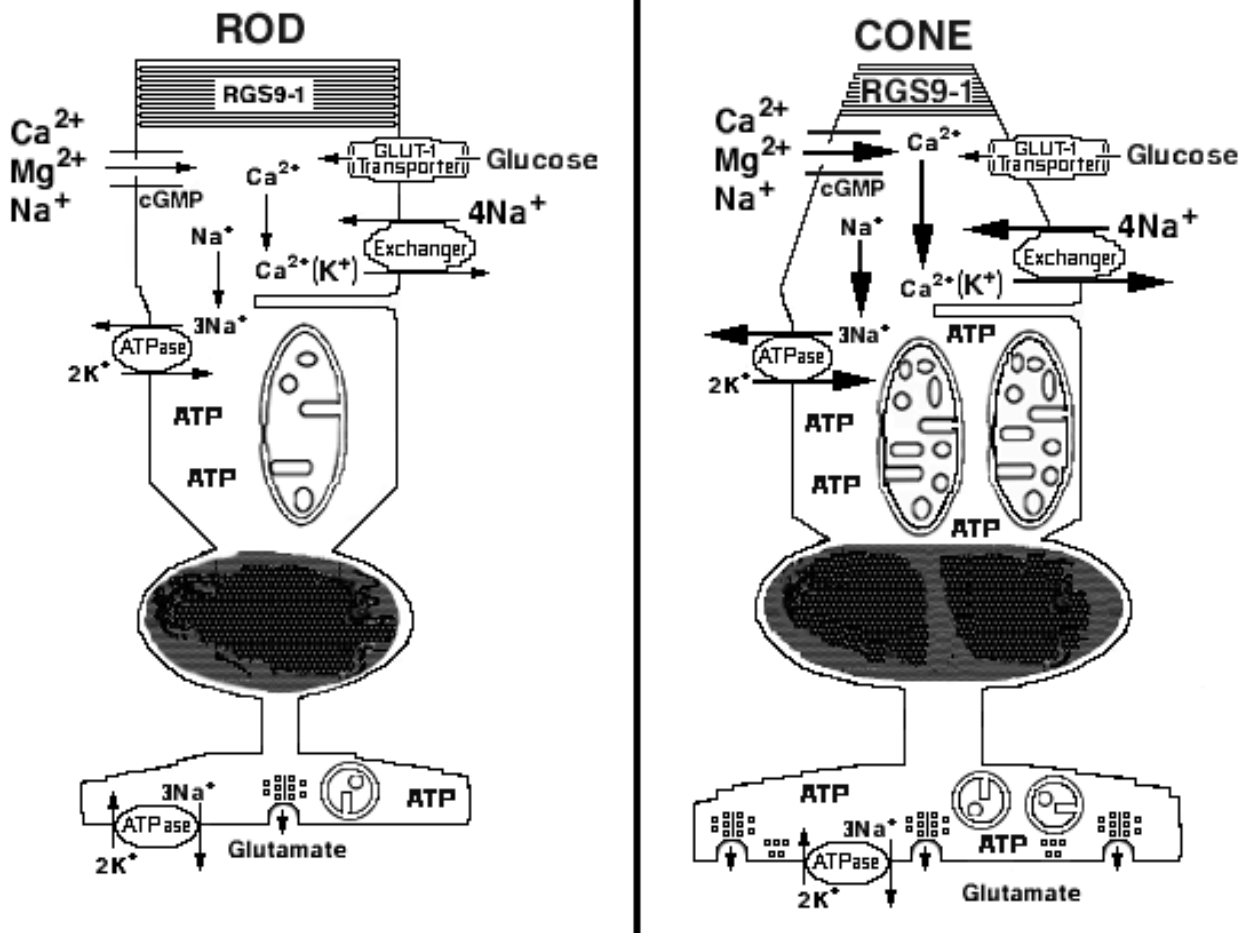

Figure 9. Light-adapted rod and cone photoreceptor. Schematic drawing of light-adapted rod and middle wavelength-sensitive (M) cone photoreceptors illustrating fundamental bioenergetic and functional differences. Outer segment: The relatively larger arrows in the cone, compared to rod, outer segments indicate the cone's higher relative permeability for Ca^{2+} through the cGMP-gated channel, higher fraction of the dark current carried by Ca^{2+} and more rapid $Na^+/Ca^{2+}(K^+)$ exchanger [15-18]. The GLUT-1-type glucose transporter appears to have similar kinetics in rod and cone outer segments [5,72]. The relatively larger lettering for RGS9-1 in cone outer segments indicates the higher content of this GTPase accelerating protein (GAP) in mouse cones, compared to rods [21,64]. Inner segment: The relatively larger arrows in the cone, compared to rod, inner segment Na^+,K^+-ATPase indicates the higher relative activity of the cones [20]. We found that mouse rods and cones in situ are in the orthodox, rather than the condensed, conformation (see text and Hackenbrock [30]). The mouse rods have an average of approximately 5 mitochondria per cell, whereas cones have approximately 10 mitochondria per cell (see text and Figure 1B). Mouse cone mitochondria also were more uniformly stained and more reactive for cytochrome c oxidase than rod mitochondria (see text and Figure 1B). Consistent with our results, cones also contain more ATP than rods [59]. The cone mitochondria had narrower crista junctions, greater cristae connectivity and approximately 3-fold more cristae membrane surface area compared to rods (see text and Figure 4, Figure 5, and Figure 6). Synaptic terminal: The rod synaptic terminal or spherule contains a single invagination of the plasma membrane where glutamate is released. The spherule contains one or two small mitochondria. The cone synaptic terminal or pedicle contains numerous invaginations as well as flat contact sites where glutamate is released. The pedicle contains several medium to large mitochondria [1,4,6-8]. The cone mitochondria are more reactive for cytochrome c oxidase than the rod mitochondria ([9,20]; unpublished data).

The retiform configuration can be thought of as a reticulum or set of multibranched cristae segments. Despite the dense packing of cristae in cone mitochondria, no tubular association was observed [80]. We found that most cristae had both lamellar and tubular segments usually with constrictions placed along their lengths. This is in contrast to the findings of Lea and Hollenberg [25] who found only tubular cristae in kidney, liver, and light-adapted retina mitochondria. This appears to be a limitation of their two-dimensional scanning EM and serial reconstruction procedures. Although some cristae were tubular throughout their length, it was rare to find a crista that was exclusively lamellar. Even though cones possess a high-energy requirement, the number of mitochondrial contact sites does not differ from that of rods. This is consistent with the observation that neither the abundance nor the area occupied by these sites appears to be dependent on the metabolic state [81]. Instead, one proposed role of contact sites is the translocation of cholesterol that is mediated by GTP binding proteins [82]. Thus, our structural results help elucidate how cone mitochondria can respire at a higher rate than do their rod counterparts.

We also discovered that the crista junction opening in CIS mitochondria is significantly smaller than that in RIS mitochondria. It has been proposed that Mgm1, a dynamin-like GTPase localized to the mitochondrial periphery mediates crista formation at crista junctions [81]. It was suggested that the second step in crista formation is the placement of a physical constraint on the diameter of these junctions [83]. Mannella et al. [38] suggested, from modeling studies, that the physical constraint might form a barrier to the free diffusion of molecules such as ADP, ATP and cytochrome c. They further suggested that the intracristal ADP concentration might be lowered due to the crista junction barrier and as such, the efficiency of ATP production would be lessened [38]. Whether the narrower junctional opening in cone mitochondria limits the rate of ATP generation and opposes the increased capacity for ATP production afforded by an abundant inner membrane is unknown and will require further investigations.

Crista junctions, defined by Perkins and co-workers [33] as the site where the cristae connect to the inner boundary membrane, have been examined and discussed in relation to normal mitochondrial function and pathological alterations during apoptosis [35,36,39,52,84-87]. Several reports have speculated that apoptosis might be related to an increase in the crista junction size [40,80]. However, our recent in vivo study showed that there were no changes in crista junction size in RIS mitochondria of rod photoreceptors undergoing developmentally lead-induced apoptosis [39]. Therefore, the importance and role that changes in crista junction size plays during various stages of the apoptosis requires further investigation.

In summary, our results demonstrate that middle wavelength (M) cones have a different bioenergetic signature than do rods and suggest that the aerobic ATP generation in cones is greater than in rods (Figure 9). Our findings are consistent with results [5,8,9,14,22,61,62] that indicate that light-adapted cones have a higher aerobic energy demand and consequent ATP production than light-adapted rods. The greater ATP production by cones may provide them increased protection against metabolic insults and apoptosis compared to rods. Finally, pharmacological and nonpharmacological treatments preserve or augment mitochondrial energy production may provide immediate and long-term benefit in a wide variety of photoreceptor and retinal diseases, injuries and metabolic disturbances.

ACKNOWLEDGEMENTS

We thank Ms. Yvonne S Blocker and Drs. Lihua He, Rick Lawrence and David Mastronarde for technical assistance and suggestions. Partially funded by NIH Grant ES03183, EY07024 and UH PEER Grant to DAF. Part of this work was performed at the National Center for Microscopy and Imaging Research supported by NIH Research Resource Grant RR04050 and NIH Grant R01 NS14718 to MHE.

REFERENCES

1. Hogan MJ, Alvarado JA, Weddell JE. Histology of the human eye; an atlas and textbook. Philadelphia: Saunders; 1971.
2. Rodrigues M, Hackett J, Wiggert B, Gery I, Spiegel A, Krishna G, Stein P, Chader G. Immunoelectron microscopic localization of photoreceptor-specific markers in the monkey retina. Curr Eye Res 1987; 6:369-80.
3. Curcio CA, Hendrickson AE. Organization and development of the primate photoreceptor mosaic. Prog Ret Res 1990; 10:89-120.
4. Djamgoz MBA, Archer SN, Vallerga S, editors. Neurobiology and clinical aspects of the outer retina. London: Chapman & Hall; 1995.
5. Molday RS. Photoreceptor membrane proteins, phototransduction, and retinal degenerative diseases. The Friedenwald Lecture. Invest Ophthalmol Vis Sci 1998; 39:2491-513.
6. Rodieck RW. The first steps in seeing. Sunderland (MA): Sinauer Associates; 1998.
7. Kaufman PL, Alm A, editors. Adler's physiology of the eye. 10th ed. St. Louis: Mosby; 2003.
8. Cohen AI. The fine structure of the extrafoveal receptors of the Rhesus monkey. Exp Eye Res 1961; 1:128-36.
9. Kageyama GH, Wong-Riley MT. The histochemical localization of cytochrome oxidase in the retina and lateral geniculate nucleus of the ferret, cat, and monkey, with particular reference to retinal mosaics and ON/OFF-center visual channels. J Neurosci 1984; 4:2445-59.
10. Chen E, Soderberg PG, Lindstrom B. Activity distribution of cytochrome oxidase in the rat retina. A quantitative histochemical study. Acta Ophthalmol (Copenh) 1989; 67:645-51.
11. Buono RJ, Sheffield JB. Changes in distribution of mitochondria in the developing chick retina. Exp Eye Res 1991; 53:187-98.
12. Medrano CJ, Fox DA. Oxygen consumption in the rat outer and inner retina: light- and pharmacologically-induced inhibition. Exp Eye Res 1995; 61:273-84.
13. Linsenmeier RA. Effects of light and darkness on oxygen distribution and consumption in the cat retina. J Gen Physiol 1986; 88:521-42.
14. Hoang QV, Linsenmeier RA, Chung CK, Curcio CA. Photoreceptor inner segments in monkey and human retina: mitochondrial density, optics, and regional variation. Vis Neurosci 2002; 19:395-407.

15. Miller JL, Korenbrot JI. Phototransduction and adaptation in rods, single cones, twin cones of the striped bass retina: a comparative study. Vis Neurosci 1993; 10:653-67.
16. Korenbrot JI. Ca2+ flux in retinal rod and cone outer segments: differences in Ca2+ selectivity of the cGMP-gated ion channels and Ca2+ clearance rates. Cell Calcium 1995; 18:285-300.
17. Picones A, Korenbrot JI. Permeability and interaction of Ca2+ with cGMP-gated ion channels differ in retinal rod and cone photoreceptors. Biophys J 1995; 69:120-7.
18. Schneeweis DM, Schnapf JL. Photovoltage of rods and cones in the macaque retina. Science 1995; 268:1053-6.
19. Bernstein SL, Wong P. Regional expression of disease-related genes in human and monkey retina. Mol Vis 1998; 4:24 .
20. Wong-Riley MT, Huang Z, Liebl W, Nie F, Xu H, Zhang C. Neurochemical organization of the macaque retina: effect of TTX on levels and gene expression of cytochrome oxidase and nitric oxide synthase and on the immunoreactivity of Na+ K+ ATPase and NMDA receptor subunit I. Vision Res 1998; 38:1455-77.
21. Cowan CW, Fariss RN, Sokal I, Palczewski K, Wensel TG. High expression levels in cones of RGS9, the predominant GTPase accelerating protein of rods. Proc Natl Acad Sci U S A 1998; 95:5351-6.
22. Yamada E. Some structural features of the fovea centralis in the human retina. Arch Ophthalmol 1969; 82:151-9.
23. Sjostrand FS. The ultrastructure of the inner segment of the retinal rods of the guinea pig eye as revealed by electron microscopy. Journal of cellular and comparative physiology 1953; 42:45-70.
24. Carter-Dawson LD, LaVail MM. Rods and cones in the mouse retina. I. Structural analysis using light and electron microscopy. J Comp Neurol 1979; 188:245-62.
25. Lea PJ, Hollenberg MJ. Mitochondrial structure revealed by high-resolution scanning electron microscopy. Am J Anat 1989; 184:245-57.
26. Sjostrand FS. Electron microscopy of mitochondria and cytoplasmic double membranes. Nature 1953; 171:30-1.
27. Baumeister W, Grimm R, Walz J. Electron tomography of molecules and cells. Trends Cell Biol 1999; 9:81-5.
28. Perkins G, Frey T. Electron tomography. In: Creighton TE, editor. Encyclopedia of molecular biology. New York: John Wiley; 1999. p. 796.
29. Frank J, Wagenknecht T, McEwen BF, Marko M, Hsieh CE, Mannella CA. Three-dimensional imaging of biological complexity. J Struct Biol 2002; 138:85-91.
30. Hackenbrock CR. Ultrastructural bases for metabolically linked mechanical activity in mitochondria. I. Reversible ultrastructural changes with change in metabolic steady state in isolated liver mitochondria. J Cell Biol 1966; 30:269-97.
31. Rasmussen N. Mitochondrial structure and the practice of cell biology in the 1950s. J Hist Biol 1995; 28:381-429.
32. Scheffler IE. A century of mitochondrial research: achievements and perspectives. Mitochondrion 2000; 1:3-31.
33. Perkins G, Renken C, Martone ME, Young SJ, Ellisman M, Frey T. Electron tomography of neuronal mitochondria: three-dimensional structure and organization of cristae and membrane contacts. J Struct Biol 1997; 119:260-72.
34. Perkins GA, Renken CW, Song JY, Frey TG, Young SJ, Lamont S, Martone ME, Lindsey S, Ellisman MH. Electron tomography of large, multicomponent biological structures. J Struct Biol 1997; 120:219-27.
35. Frey TG, Mannella CA. The internal structure of mitochondria. Trends Biochem Sci 2000; 25:319-24.
36. Perkins GA, Frey TG. Recent structural insight into mitochondria gained by microscopy. Micron 2000; 31:97-111.
37. Lutter M, Perkins GA, Wang X. The pro-apoptotic Bcl-2 family member tBid localizes to mitochondrial contact sites. BMC Cell Biol 2001; 2:22.
38. Mannella CA, Pfeiffer DR, Bradshaw PC, Morau II, Slepchenko B, Loew LM, Hsieh CE, Buttle K, Marko M. Topology of the mitochondrial inner membrane: dynamics and bioenergetic implications. IUBMB Life 2001; 52:93-100.
39. He L, Perkins GA, Poblenz AT, Harris JB, Hung M, Ellisman MH, Fox DA. Bcl-xL overexpression blocks bax-mediated contact site formation and apoptosis in rod photoreceptors of lead-exposed mice. Proc Natl Acad Sci U S A 2003; 100:1022-7.
40. Scorrano L, Ashiya M, Buttle K, Weiler S, Oakes SA, Mannella CA, Korsmeyer SJ. A distinct pathway remodels mitochondrial cristae and mobilizes cytochrome c during apoptosis. Dev Cell 2002; 2:55-67.
41. Fox DA, Chu LW. Rods are selectively altered by lead: II. Ultrastructure and quantitative histology. Exp Eye Res 1988; 46:613-25.
42. Fox DA, Campbell ML, Blocker YS. Functional alterations and apoptotic cell death in the retina following developmental or adult lead exposure. Neurotoxicology 1997; 18:645-64.
43. He L, Poblenz AT, Medrano CJ, Fox DA. Lead and calcium produce rod photoreceptor cell apoptosis by opening the mitochondrial permeability transition pore. J Biol Chem 2000; 275:12175-84.
44. Kueng-Hitz N, Grimm C, Lansel N, Hafezi F, He L, Fox DA, Reme CE, Niemeyer G, Wenzel A. The retina of c-fos-/- mice: electrophysiologic, morphologic and biochemical aspects. Invest Ophthalmol Vis Sci 2000; 41:909-16.
45. Szel A, Rohlich P, Caffe AR, Juliusson B, Aguirre G, Van Veen T. Unique topographic separation of two spectral classes of cones in the mouse retina. J Comp Neurol 1992; 325:327-42.
46. Jacobs GH, Fenwick JA, Williams GA. Cone-based vision of rats for ultraviolet and visible lights. J Exp Biol 2001; 204:2439-46.
47. He L, Campbell ML, Srivastava D, Blocker YS, Harris JR, Swaroop A, Fox DA. Spatial and temporal expression of AP-1 responsive rod photoreceptor genes and bZIP transcription factors during development of the rat retina. Mol Vis 1998; 4:32 .
48. Wong-Riley M. Changes in the visual system of monocularly sutured or enucleated cats demonstrable with cytochrome oxidase histochemistry. Brain Res 1979; 171:11-28.
49. Shulman LM, Fox DA. Dopamine inhibits mammalian photoreceptor Na+,K+-ATPase activity via a selective effect on the alpha3 isozyme. Proc Natl Acad Sci U S A 1996; 93:8034-9.
50. Mastronarde DN. Dual-axis tomography: an approach with alignment methods that preserve resolution. J Struct Biol 1997; 120:343-52.
51. Ahmed J, Braun RD, Dunn R Jr, Linsenmeier RA. Oxygen distribution in the macaque retina. Invest Ophthalmol Vis Sci 1993; 34:516-21.
52. Perkins GA, Renken CW, Frey TG, Ellisman MH. Membrane architecture of mitochondria in neurons of the central nervous system. J Neurosci Res 2001; 66:857-65.
53. Mannella CA, Marko M, Penczek P, Barnard D, Frank J. The internal compartmentation of rat-liver mitochondria: tomographic study using the high-voltage transmission electron microscope. Microsc Res Tech 1994; 27:278-83.
54. Mannella CA, Marko M, Buttle K. Reconsidering mitochondrial structure: new views of an old organelle. Trends Biochem Sci 1997; 22:37-8.

55. Medrano CJ, Fox DA. Substrate-dependent effects of calcium on rat retinal mitochondrial respiration: physiological and toxicological studies. Toxicol Appl Pharmacol 1994; 125:309-21.
56. McIntosh JR. Electron microscopy of cells: a new beginning for a new century. J Cell Biol 2001; 153:F25-32.
57. Smith RA, Ord MJ. Mitochondrial form and function relationships in vivo: their potential in toxicology and pathology. Int Rev Cytol 1983; 83:63-134.
58. Kadenbach B, Barth J, Akgun R, Freund R, Linder D, Possekel S. Regulation of mitochondrial energy generation in health and disease. Biochim Biophys Acta 1995; 1271:103-9.
59. Scarpelli DG, Craig EL. The fine localization of nucleoside triphosphatase activity in the retina of the frog. J Cell Biol 1963; 17:279-88.
60. Winkler BS. Glycolytic and oxidative metabolism in relation to retinal function. J Gen Physiol 1981; 77:667-92.
61. Ames A 3rd, Walseth TF, Heyman RA, Barad M, Graeff RM, Goldberg ND. Light-induced increases in cGMP metabolic flux correspond with electrical responses of photoreceptors. J Biol Chem 1986; 261:13034-42.
62. Hsu SC, Molday RS. Glucose metabolism in photoreceptor outer segments. Its role in phototransduction and in NADPH-requiring reactions. J Biol Chem 1994; 269:17954-9.
63. Palczewski K, Saari JC. Activation and inactivation steps in the visual transduction pathway. Curr Opin Neurobiol 1997; 7:500-4.
64. Lyubarsky AL, Naarendorp F, Zhang X, Wensel T, Simon MI, Pugh EN Jr. RGS9-1 is required for normal inactivation of mouse cone phototransduction. Mol Vis 2001; 7:71-8 .
65. Kaupp UB, Seifert R. Cyclic nucleotide-gated ion channels. Physiol Rev 2002; 82:769-824.
66. Wallimann T, Wegmann G, Moser H, Huber R, Eppenberger HM. High content of creatine kinase in chicken retina: compartmentalized localization of creatine kinase isoenzymes in photoreceptor cells. Proc Natl Acad Sci U S A 1986; 83:3816-9.
67. Musser GI, Rosen S. Carbonic anhydrase activity in primate photoreceptors. Exp Eye Res 1973; 15:467-70.
68. Nork MT, McCormick SA, Chao GM, Odom JV. Distribution of carbonic anhydrase among human photoreceptors. Invest Ophthalmol Vis Sci 1990; 31:1451-8.
69. Ames A 3rd, Li YY, Heher EC, Kimble CR. Energy metabolism of rabbit retina as related to function: high cost of Na+ transport. J Neurosci 1992; 12:840-53.
70. Noell WK. Aspects of experimental and hereditary retinal degeneration. In: Graymore CN, editor. Biochemistry of the retina. London: Academic Press; 1965. p. 51-72.
71. Lowry OH, Roberts NR, Schulz DW, Clow JE, Clark JR. Quantitative histochemistry of retina. II. Enzymes of glucose metabolism. J Biol Chem 1961; 236:2813-20.
72. Hsu SC, Molday RS. Glycolytic enzymes and a GLUT-1 glucose transporter in the outer segments of rod and cone photoreceptor cells. J Biol Chem 1991; 266:21745-52.
73. Nihira M, Anderson K, Gorin FA, Burns MS. Primate rod and cone photoreceptors may differ in glucose accessibility. Invest Ophthalmol Vis Sci 1995; 36:1259-70.
74. Macaluso C, Onoe S, Niemeyer G. Changes in glucose level affect rod function more than cone function in the isolated, perfused cat eye. Invest Ophthalmol Vis Sci 1992; 33:2798-808.
75. Ishikawa T, Pei YF. Intramitochondrial glycogen particles in rat retinal receptor cells. J Cell Biol 1965; 25:402-7.
76. Sosula L, Beaumont P, Hollows FC, Jonson KM, Regtop HL. Glycogen accumulation in retinal neurons and glial cells of streptozotocin-diabetic rats. Quantitative electron microscopy. Diabetes 1974; 23:221-31.
77. Kaiser-Kupfer MI, Ludwig IH, de Monasterio FM, Valle D, Krieger I. Gyrate atrophy of the choroid and retina. Early findings. Ophthalmology 1985; 92:394-401.
78. Murphy MP, Smith RA. Drug delivery to mitochondria: the key to mitochondrial medicine. Adv Drug Deliv Rev 2000; 41:235-50.
79. Gold DR, Cohen BH. Treatment of mitochondrial cytopathies. Semin Neurol 2001; 21:309-25.

The print version of this article was created on 11 Mar 2003. This reflects all typographical corrections and errata to the article through that date. Details of any changes may be found in the online version of the article.